Mid-infrared subwavelength modulator based on grating-assisted coupling of a hybrid plasmonic waveguide mode to a graphene plasmon – Supplementary Information

Yonghan Kim and Min-Suk Kwon

School of Electrical and Computer Engineering, Ulsan National Institute of Science and Technology

50 UNIST-gil, Ulju-gun, Ulsan 689-798, Korea

E-mail addresses

Yonghan kim: kodrick@unist.ac.kr

Min-Suk Kwon: mskwon@unist.ac.kr

Corresponding author: Min-Suk Kwon

Tel: +82 52 2172135

Fax: +82 52 2172130

S1. Analysis based on coupled mode equations

There is a waveguide which supports two waveguide modes propagating along the z axis: mode a and mode b. The propagation constant and attenuation coefficient of mode a (b) are β_a and α_a (β_b and α_b), respectively. The amplitudes of modes a and b are $A(z)$ and $B(z)$, respectively. If the waveguide is uniform in the z-axis, $A(z)$ and $B(z)$ are just constant. Co-directional coupling between the two modes occurs when a periodic perturbation or grating of period Λ exists in the waveguide. If the perturbation is weak, $A(z)$ and $B(z)$ are determined by the coupled mode equations:

$$\frac{dA}{dz} = i\kappa B e^{-(\alpha_b-\alpha_a)z} e^{i\delta z}, \tag{S1}$$

$$\frac{dB}{dz} = i\kappa A e^{(\alpha_b-\alpha_a)z} e^{-i\delta z}, \tag{S2}$$

where κ is a coupling coefficient and δ is the phase mismatch factor given by $\beta_b - \beta_a - 2\pi/\Lambda$. It is assumed that $\beta_b > \beta_a$ and $\alpha_b >> \alpha_a$. In addition, it is assumed that $A(0) = 1$ and $B(0) = 0$. α represents $\alpha_b - \alpha_a$.

When the phase-matching condition is satisfied (*i.e.*, $\delta = 0$) and $\kappa > \alpha/2$, the coupled mode equations are solved such that

$$A(z) = e^{-\alpha z/2}\left[\cos(\bar{\kappa}z) + \frac{\alpha}{2\bar{\kappa}}\sin(\bar{\kappa}z)\right], \tag{S3}$$

$$B(z) = i\frac{\kappa}{\bar{\kappa}} e^{\alpha z/2}\sin(\bar{\kappa}z). \tag{S4}$$

where $\bar{\kappa} = \sqrt{\kappa^2 - (\alpha/2)^2}$. The power of mode a, $P_a(z)$ and the power of mode b, $P_b(z)$ are given by

$$P_a(z) = e^{-\bar{\alpha}z}\left[\cos(\bar{\kappa}z) + \frac{\alpha}{2\bar{\kappa}}\sin(\bar{\kappa}z)\right]^2, \tag{S5}$$

$$P_b(z) = e^{-\bar{\alpha}z}\left(\frac{\kappa}{\bar{\kappa}}\right)^2 \sin^2(\bar{\kappa}z), \tag{S6}$$

where $\bar{\alpha} = \alpha_b + \alpha_a$.

When $\delta = 0$ and $\kappa < \alpha/2$, the coupled mode equations are solved such that

$$A(z) = \frac{\alpha''}{\alpha'' - \alpha'} e^{-\alpha' z/2} - \frac{\alpha'}{\alpha'' - \alpha'} e^{-\alpha'' z/2}, \tag{S7}$$

$$B(z) = \frac{i}{2\kappa} \frac{\alpha'\alpha''}{\alpha'' - \alpha'} e^{\alpha z} (e^{-\alpha' z/2} - e^{-\alpha'' z/2}), \tag{S8}$$

where $\alpha' = \alpha/2 - \sqrt{(\alpha/2)^2 - \kappa^2}$ and $\alpha'' = \alpha/2 + \sqrt{(\alpha/2)^2 - \kappa^2}$. $P_a(z)$ and $P_b(z)$ are given by

$$P_a(z) = e^{-2\alpha_a z} \left(\frac{\alpha''}{\alpha'' - \alpha'} e^{-\alpha' z/2} - \frac{\alpha'}{\alpha'' - \alpha'} e^{-\alpha'' z/2} \right)^2, \tag{S9}$$

$$P_b(z) = \frac{1}{4\kappa^2} \left(\frac{\alpha'\alpha''}{\alpha'' - \alpha'} \right)^2 e^{-2\alpha_a z} (e^{-\alpha' z/2} - e^{-\alpha'' z/2})^2. \tag{S10}$$

When α_a = 0.0025 μm^{-1} and α_b = 0.5 μm^{-1}, $P_a(z)$ and $P_b(z)$ were calculated for a few values of κ and they are shown in Figure S1. If κ is sufficiently large, P_a becomes equal to zero at some distance, and P_b first increases and then decreases within that distance. However, if κ is much smaller than α, P_a slowly decreases from 1 as z increases, and P_b is almost equal to zero. This can be confirmed from Equations S9 and S10. If $\kappa << \alpha/2$, $\alpha' \approx 0$ and $\alpha'' \approx \alpha$. Then, $P_a(z) \approx e^{-2\alpha_a z}$, and $P_b(z) \approx 0$. Therefore, for the power of mode a to decrease to zero at some distance, κ must be larger than $\alpha/2$. Since κ is determined by a modal overlap between modes a and b in the perturbed region, the overlap must be intense for the efficient co-directional coupling of mode a to mode b if α_b is very large. This is satisfied by the hybrid plasmonic waveguide, the HPWM and the GPWM of which correspond to mode a and mode b, respectively.

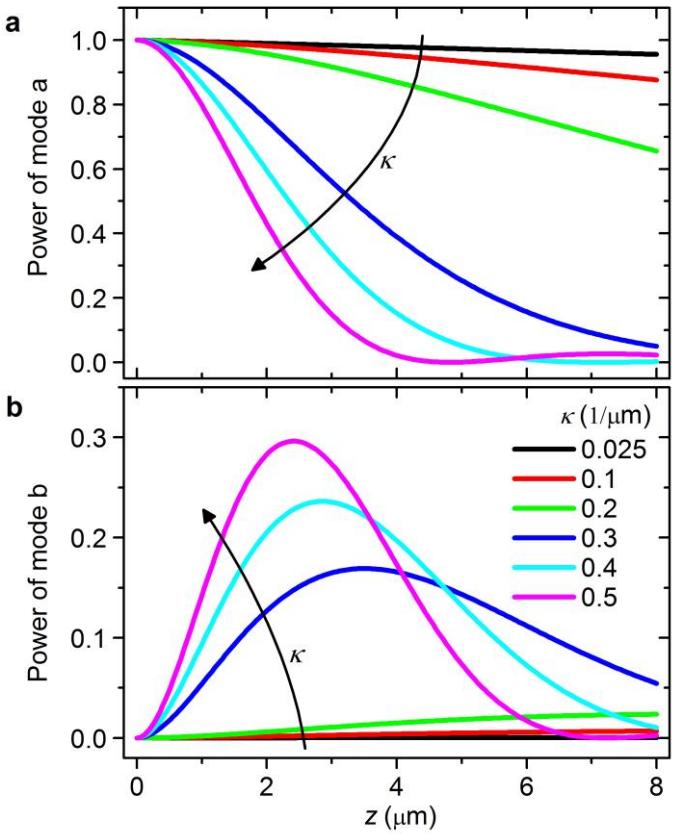

Figure S1. (a) Change of the power of mode a along the grating. (b) Change of the power of mode b along the grating.

It can be estimated how strongly mode a should be confined in the perturbed region when mode b is the graphene plasmon polariton (GPP) of the graphene embedded in a homogeneous medium of refractive index n. The magnetic field of the GPP, $H_b(x)$ is given by

$$H_b(x) = \sqrt{\frac{2n^2 k_0 \xi_b}{\eta_0 \gamma_b} P} \times \begin{cases} \exp(-\xi_b x), & x > 0, \\ \exp(\xi_b x), & x < 0, \end{cases} \tag{S11}$$

where $k_0 = 2\pi/\lambda$ and $\eta_0 = \sqrt{\mu_0 / \varepsilon_0}$. In addition, $\gamma_b = \beta_b + i\alpha_b$, and $\xi_b = \sqrt{\gamma_b^2 - k_0^2 n^2}$ whose real part is chosen to be positive. P is a sort of mode power calculated by using Equation (S27), which is usually 1 W/μm. The perturbed region is between $x = 0$ and $x = -d_g$, and it is assumed that the magnetic field of mode a is almost constant since the region is actually much narrower than the effective mode width of mode a. If the fraction of the power of mode a in the perturbed region is Γ_a, the magnetic field of mode a in the region, H_a is approximately given by

$$H_a = \sqrt{\frac{2n^2 k_0}{\eta_0 \gamma_a d_g} \Gamma_a P}, \tag{S12}$$

where $\gamma_a = \beta_a + i\alpha_a$. Then, the coupling coefficient K(z) between modes a and b is given by

$$\begin{aligned} \mathrm{K}(z) &= -i \frac{\eta_0}{4k_0} \frac{\Delta n^2(z)}{n^4} \frac{\gamma_a \gamma_b}{P} \int_{-d_g}^{0} H_a H_b(x) dx, \\ &\approx -i \frac{\Delta n^2(z)}{2n^2} \sqrt{\frac{\gamma_a \gamma_b}{d_g} \Gamma_a} \sqrt{\xi_b} \int_{-\infty}^{0} \exp(\xi_b x) dx, \\ &= -i \frac{\Delta n^2(z)}{2n^2} \sqrt{\frac{\gamma_a \gamma_b}{d_g \xi_b} \Gamma_a}, \\ &\approx -i \frac{\Delta n^2(z)}{2n^2} \sqrt{\frac{\gamma_a}{d_g} \Gamma_a}, \end{aligned} \tag{S13}$$

where $\Delta n^2(z)$ represents the change of n^2 along the grating. For the grating formed by air grooves, $\Delta n^2(z)$ alternates between 0 and $n^2 - 1$. The second approximation is valid if $d_g >> 1/\xi_b$, and the last approximation is valid since γ_b is almost the same as ξ_b for the GPP. κ in Equations (S1) to (S10) is obtained from the Fourier series expansion of K(z) and hence smaller than $K_{max} = (n^2 - 1)/(2n^2)\sqrt{|\gamma_a| \Gamma_a / d_g}$. When n = 2.22 (the refractive index of ZnS at 8 μm), $|\gamma_a| \approx \beta_a$ = 3.26 × k_0 (the propagation constant of the HPWM in section 1 at 8 μm), and d_g = 70 nm, Γ_a should be larger than 4.3 % for K_{max} > 0.5 μm^{-1}. The actual value of Γ_a of the HPWM in section 1 is 4.8 %. (For reference, in the case of the photonic waveguide, which is the hybrid plasmonic waveguide with the metal replaced by air, the fraction of the power of its fundamental TM mode in the perturbed region is just 0.07 %. This shows that Γ_a of the HPWM is exceptionally large.) Therefore, we can conclude that the HPWM is confined in the perturbed region as strongly as required for a sufficiently large value of κ. Last, it is necessary to note that the validity of the analysis based on the coupled mode equations is limited since the perturbation given by the grating is not weak. Therefore, the modulator should be analyzed by using a more rigorous method.

S2. Waveguide analysis based on the transfer matrix method

A multilayer waveguide is schematically shown in Figure S2. It is uniform in the y-axis and has L+1 boundaries. The boundary at $x = x_l$, $l = 0, 1, \ldots, L$, has a surface conductivity σ_l such that there is a surface current density given by $\sigma_l \mathbf{E}_t(x_l)$, where $\mathbf{E}_t$ represents the electric field component normal to the x-axis. A transverse magnetic (TM) mode has a magnetic field $\mathbf{H}(x, z, t) = \hat{\mathbf{y}} H(x)\exp(i\gamma z - i\omega t)$, where $\gamma = \beta + i\alpha$ and β and α are the propagation constant and attenuation coefficient of the mode. From the Helmholtz equation, it is found that

$$H(x) = H_0 \times \begin{cases} \psi_{L+1} \dfrac{k_0 n_{L+1}^2}{i\kappa_{L+1}} \exp[i\kappa_{L+1}(x - x_L)], & x > x_L, \\ \phi_l \cos[\kappa_l (x - x_{l-1})] + \psi_l \dfrac{k_0 n_l^2}{\kappa_l} \sin[\kappa_l (x - x_{l-1})], & x_{l-1} < x < x_l, \quad l = 1, \cdots, L, \\ \exp[-i\kappa_0 (x - x_0)], & x < x_0, \end{cases} \tag{S14}$$

where $k_0 = 2\pi/\lambda$ and $\kappa_l = \sqrt{(k_0 n_l)^2 - \gamma^2}$. The imaginary parts of κ_0 and κ_{L+1} have to be positive. Using the boundary conditions that

$$\frac{1}{n_l^2} \frac{dH}{dx}\bigg|_{x=x_l^-} = \frac{1}{n_{l+1}^2} \frac{dH}{dx}\bigg|_{x=x_l^+}, \tag{S15}$$

$$H(x_l^+) - H(x_l^-) = \frac{i\sigma_l \eta_0}{k_0 n_l^2} \frac{dH}{dx}\bigg|_{x=x_l^-}, \tag{S16}$$

where x_l^+ (x_l^-) is infinitesimally larger (smaller) than x_l and $\eta_0 = \sqrt{\mu_0 / \varepsilon_0}$, the transfer matrix M_l is determined. The matrix equation for (ϕ_l, ψ_l) is

$$\begin{bmatrix} \phi_{l+1} \\ \psi_{l+1} \end{bmatrix} = M_l \begin{bmatrix} \phi_l \\ \psi_l \end{bmatrix} = \begin{bmatrix} m_{l,11} & m_{l,12} \\ m_{l,21} & m_{l,22} \end{bmatrix} \begin{bmatrix} \phi_l \\ \psi_l \end{bmatrix}, \; l = 1, \cdots, L, \text{ and } \begin{bmatrix} \phi_1 \\ \psi_1 \end{bmatrix} = \begin{bmatrix} 1 + \sigma_0 \eta_0 \kappa_0 / (k_0 n_0^2) \\ -i\kappa_0 / (k_0 n_0^2) \end{bmatrix}, \tag{S17}$$

$$m_{l,11} = \cos(\kappa_l d_l) - i\sigma_l \eta_0 \frac{\kappa_l}{k_0 n_l^2} \sin(\kappa_l d_l), \tag{S18}$$

$$m_{l,12} = \frac{k_0 n_l^2}{\kappa_l} \sin(\kappa_l d_l) + i\sigma_l \eta_0 \cos(\kappa_l d_l), \tag{S19}$$

$$m_{l,21} = -\frac{\kappa_l}{k_0 n_l^2} \sin(\kappa_l d_l), \tag{S20}$$

$$m_{l,22} = \cos(\kappa_l d_l), \tag{S21}$$

where $d_l = x_l - x_{l-1}$. Finally, the characteristic equation for γ is

$$\phi_{L+1} + i\frac{k_0 n_{L+1}^2}{\kappa_{L+1}}\psi_{L+1} = 0. \tag{S22}$$

γ is determined by numerically finding the roots of Equation (S22).

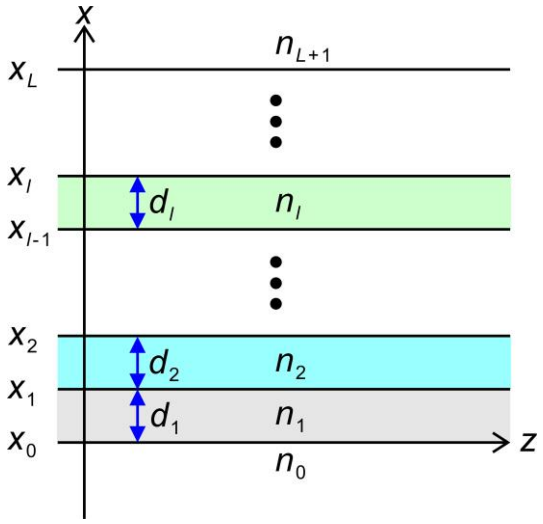

Figure S2. Structure of a multilayer waveguide. The boundary at $x = x_l$, $l = 0, 1, \ldots, L$, has a surface conductivity σ_l.

S3. Mode matching method

The mode matching method used in this work is based on Ref S1. There is the interface between two waveguides (Figure S3). A waveguide mode of order m of the left waveguide has the electric field $\mathbf{E}_m^L(x,y)\exp(-i\gamma_m^L z)$ and the magnetic field $\mathbf{H}_m^L(x,y)\exp(-i\gamma_m^L z)$ (γ_m^L is the complex propagation constant of the mode of order m). Similarly, a waveguide mode of order n of the right waveguide has the electric field $\mathbf{E}_n^R(x,y)\exp(-i\gamma_n^R z)$ and the magnetic field $\mathbf{H}_n^R(x,y)\exp(-i\gamma_n^R z)$ (γ_n^R is the complex propagation constant of the mode of order n). When the left waveguide mode of order m is incident on the interface, it is partially coupled to the left-going modes of the left waveguide and partially coupled to the right-going modes of the right waveguide. The mode matching at the interface makes the reflection and transmission of the incident mode expressed by

$$\mathbf{E}_{m,t}^L + \sum\nolimits_n r_{n,m}\mathbf{E}_{n,t}^L = \sum\nolimits_n t_{n,m}\mathbf{E}_{n,t}^R, \tag{S23}$$

$$\mathbf{H}_{m,t}^{L} - \sum_n r_{n,m}\mathbf{H}_{n,t}^{L} = \sum_n t_{n,m}\mathbf{H}_{n,t}^{R}, \tag{S24}$$

where the subscript t means the transversal component of the field. By applying the unconjugated orthogonality relation, Equations (S23) and (S24) are transformed into

$$\delta_{jm} + r_{j,m} = \sum_n t_{n,m} \left\langle \mathbf{E}_{n,t}^{R}, \mathbf{H}_{j,t}^{L} \right\rangle, \tag{S25}$$

$$\delta_{jm} - r_{j,m} = \sum_n t_{n,m} \left\langle \mathbf{E}_{j,t}^{L}, \mathbf{H}_{n,t}^{R} \right\rangle, \tag{S26}$$

where $\left\langle \mathbf{E}, \mathbf{H} \right\rangle = \frac{1}{2}\int \mathbf{E} \times \mathbf{H} \cdot \hat{\mathbf{z}}\, ds$ and δ_{jm} is the Kronecker delta. The unconjugated orthogonality means

$$\left\langle \mathbf{E}_{m}^{L(R)}, \mathbf{H}_{n}^{L(R)} \right\rangle = \frac{1}{2}\int \mathbf{E}_{m}^{L(R)} \times \mathbf{H}_{n}^{L(R)} \cdot \hat{\mathbf{z}}\, ds = \frac{1}{2}\int \mathbf{E}_{m,t}^{L(R)} \times \mathbf{H}_{n,t}^{L(R)} \cdot \hat{\mathbf{z}}\, ds = \delta_{mn}. \tag{S27}$$

From Equations (S25) and (S26), the transmission matrix $\mathbf{T}_{LR}$ with the elements $\{t_{n,m}\}$ and the reflection matrix $\mathbf{R}_{LR}$ with the elements $\{r_{n,m}\}$ are determined such that

$$\mathbf{T}_{LR} = 2(\mathbf{O}_{LR} + \mathbf{O}_{RL}^{T})^{-1}, \tag{S28}$$

$$\mathbf{R}_{LR} = \frac{1}{2}(\mathbf{O}_{RL}^{T} - \mathbf{O}_{LR})\mathbf{T}_{LR}, \tag{S29}$$

where the (m, n) element of $\mathbf{O}_{LR}$ is $\left\langle \mathbf{E}_{m,t}^{L}, \mathbf{H}_{n,t}^{R} \right\rangle$ and the (m, n) element of $\mathbf{O}_{RL}$ is $\left\langle \mathbf{E}_{m,t}^{R}, \mathbf{H}_{n,t}^{L} \right\rangle$. If the waveguides are multilayer waveguides which are uniform in the y-direction and transverse magnetic (TM) polarization is considered,

$$\left\langle \mathbf{E}_{m,t}^{L}, \mathbf{H}_{n,t}^{R} \right\rangle = \frac{\gamma_m^{L}}{2\omega\varepsilon_0}\int_{-\infty}^{\infty} \frac{1}{n_L^2(x)} H_m^{L}(x) H_n^{R}(x) dx, \tag{S30}$$

$$\left\langle \mathbf{E}_{m,t}^{R}, \mathbf{H}_{n,t}^{L} \right\rangle = \frac{\gamma_m^{R}}{2\omega\varepsilon_0}\int_{-\infty}^{\infty} \frac{1}{n_R^2(x)} H_m^{R}(x) H_n^{L}(x) dx, \tag{S31}$$

where $n_L(x)$ and $n_R(x)$ are the refractive index distributions in the left and right waveguides, respectively. When $\mathbf{T}_{RL}$ represents the transmission matrix from the right waveguide to the left waveguide and $\mathbf{R}_{RL}$ represents the reflection in the right waveguide, they are given by

$$\mathbf{T}_{RL} = \mathbf{T}_{LR}^{T}, \tag{S32}$$

$$\mathbf{R}_{RL} = \frac{1}{2}(-\mathbf{O}_{RL} + \mathbf{O}_{LR}^{T})\mathbf{T}_{RL}. \tag{S33}$$

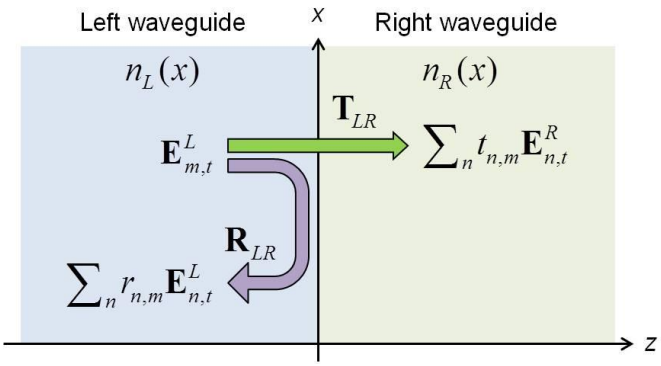

Figure S3. Interface between two waveguides. The incident mode of the left waveguide is reflected to the left waveguide modes or transmitted to the right waveguide modes.

There is a structure consisting of concatenated N waveguides (Figure S4). The h-th waveguide of this structure is located between z_{h-1} and z_h, and its length l_h is $z_h - z_{h-1}$. The complex propagation constant of the m-th order mode of the waveguide is γ_m^h. $\mathbf{F}_h$ and $\mathbf{B}_h$ are the column vectors of the amplitudes of the forward-going and backward-going modes at z_h^- (z_h^- is infinitesimally smaller than z_h). Then, the following matrix equation can be found:

$$\begin{bmatrix} \mathbf{F}_h \\ \mathbf{B}_{h-1} \end{bmatrix} = \begin{bmatrix} \mathbf{T}_F^h & \mathbf{R}_B^h \\ \mathbf{R}_F^h & \mathbf{T}_B^h \end{bmatrix} \begin{bmatrix} \mathbf{F}_{h-1} \\ \mathbf{B}_h \end{bmatrix}, \tag{S34}$$

$$\mathbf{T}_F^h = \mathrm{diag}(e^{i\gamma_m^h l_h})\mathbf{T}_{LR}^{h-1}, \tag{S35}$$

$$\mathbf{R}_B^h = \mathrm{diag}(e^{i\gamma_m^h l_h})\mathbf{R}_{RL}^{h-1}\mathrm{diag}(e^{i\gamma_m^h l_h}), \tag{S36}$$

$$\mathbf{R}_F^h = \mathbf{R}_{LR}^{h-1}, \tag{S37}$$

$$\mathbf{T}_B^h = \mathbf{T}_{RL}^{h-1}\mathrm{diag}(e^{i\gamma_m^h l_h}), \tag{S38}$$

where $\mathbf{T}_{LR}^{h-1}$, $\mathbf{R}_{LR}^{h-1}$, $\mathbf{R}_{LR}^{h-1}$, and $\mathbf{R}_{RL}^{h-1}$ are $\mathbf{T}_{LR}$, $\mathbf{R}_{LR}$, $\mathbf{T}_{RL}$, and $\mathbf{R}_{RL}$ at $z = z_{h-1}$, respectively. In addition, $\mathrm{diag}(e^{i\gamma_m^h l_h})$ is the diagonal matrix whose (m, m) element is $e^{i\gamma_m^h l_h}$. When the relation of $[\mathbf{F}_p, \mathbf{B}_1]$ to $[\mathbf{F}_1, \mathbf{B}_p]$ is given by

$$\begin{bmatrix} \mathbf{F}_p \\ \mathbf{B}_1 \end{bmatrix} = \begin{bmatrix} \mathbf{T}_{1,p} & \mathbf{R}_{p,1} \\ \mathbf{R}_{1,p} & \mathbf{T}_{p,1} \end{bmatrix} \begin{bmatrix} \mathbf{F}_1 \\ \mathbf{B}_p \end{bmatrix}, \tag{S39}$$

$\mathbf{T}_{1,p+1}$, $\mathbf{R}_{1,p+1}$, $\mathbf{T}_{p+1,1}$, and $\mathbf{R}_{p+1,1}$ for the relation of $[\mathbf{F}_{p+1}, \mathbf{B}_1]$ to $[\mathbf{F}_1, \mathbf{B}_{p+1}]$ are given by

$$\mathbf{T}_{1,p+1} = \mathbf{T}_F^{p+1}(\mathbf{I} - \mathbf{R}_{p,1}\mathbf{R}_F^{p+1})^{-1}\mathbf{T}_{1,p}, \tag{S40}$$

$$\mathbf{R}_{p+1,1} = \mathbf{T}_F^{p+1}(\mathbf{I} - \mathbf{R}_{p,1}\mathbf{R}_F^{p+1})^{-1}\mathbf{R}_{p,1}\mathbf{T}_B^{p+1} + \mathbf{R}_B^{p+1}, \tag{S41}$$

$$\mathbf{R}_{1,p+1} = \mathbf{T}_{p,1}(\mathbf{I} - \mathbf{R}_F^{p+1}\mathbf{R}_{p,1})^{-1}\mathbf{R}_F^{p+1}\mathbf{T}_{1,p} + \mathbf{R}_{1,p}, \tag{S42}$$

$$\mathbf{T}_{p+1,1} = \mathbf{T}_{p,1}(\mathbf{I} - \mathbf{R}_F^{p+1}\mathbf{R}_{p,1})^{-1}\mathbf{T}_B^{p+1}, \tag{S43}$$

where **I** is the identity matrix. Based on Equations (S39) – (S43), the relation of [$\mathbf{F}_N$, $\mathbf{B}_1$] to [$\mathbf{F}_1$, $\mathbf{B}_N$] can be found, and the transmission through the structure and the reflection from the structure can be determined. This is the mode matching method used in this work.

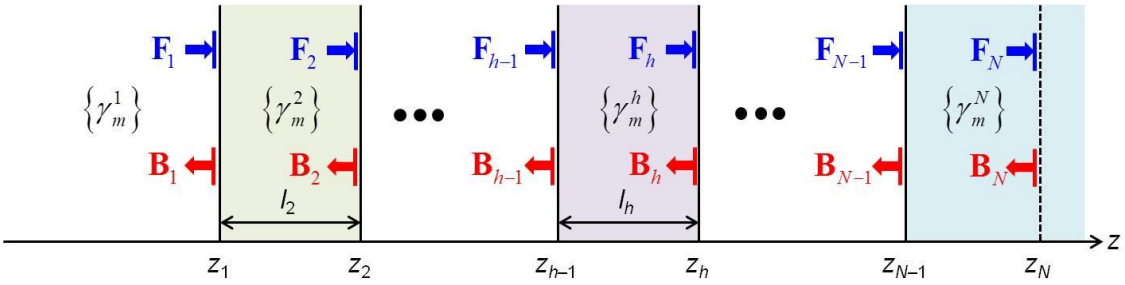

Figure S4. Schematic diagram of a structure consisting of concatenated N waveguides.

The mode matching method yields correct results when not only the guided modes of constituent waveguides but also their radiation modes are considered. The radiation modes can be so called discretized by bounding the waveguides with perfect electric conductors. However, for convenience, only the guided modes of the hybrid plasmonic waveguide are considered in this work. In addition to the HPWM and the GPWM, the hybrid plasmonic waveguide supports another guided mode which has the electric field distribution shown in Figure S5. With the HPWM launched before the grating region, the mode matching method considering the three guided modes was used to calculate the transmission from the HPWM before the grating region to that after the grating region. The calculated transmission spectrum is shown in Figure 3a.

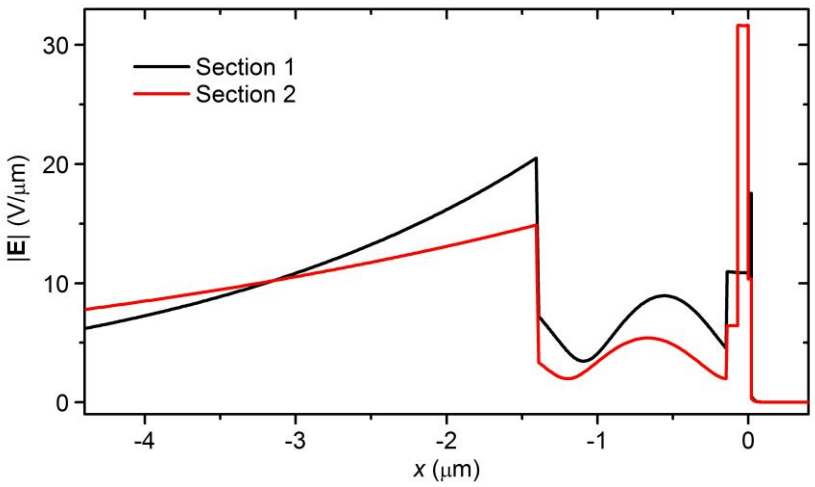

Figure S5. Electric field distributions of another guided mode in sections 1 and 2.

S4. Information about the analysis based on the FDTD method

When the FDTD method was used, the meshes used in the slot region had dimensions of 1 nm by 1 nm. The meshes used outside the slot region were gradually enlarged such that the largest meshes had dimensions of 10 nm and 8 nm in the horizontal and vertical directions, respectively. For the analysis based on the FDTD method, the fundamental TM mode was launched as a source in the input photonic waveguide, and the mode expansion monitor of FDTD Solutions was employed in the output photonic waveguide to extract the output fundamental TM mode power.

Since the hybrid plasmonic waveguide contains metal and graphene, the powers of the HPWM and the GPWM at a position in the hybrid plasmonic waveguide cannot be correctly calculated by using the mode expansion monitor. Hence, the powers were calculated by using the following steps. First, the electromagnetic fields $\mathbf{E}(x)$ and $\mathbf{H}(x)$ at the position are monitored. The transversal components of $\mathbf{E}(x)$ and $\mathbf{H}(x)$ are expanded into the sums of the transversal components of $\mathbf{E}_m(x)$ and $\mathbf{H}_m(x)$ of the modes of the hybrid plasmonic waveguide such that

$$\mathbf{E}_t = \sum C_m \mathbf{E}_{m,t} \text{ and } \mathbf{H}_t = \sum C_m \mathbf{H}_{m,t}. \tag{S44}$$

Actually, $\mathbf{H}_{m,t} = \mathbf{H}_m = \hat{\mathbf{y}} H_m$, and $\mathbf{E}_{m,t} = \hat{\mathbf{x}} E_{m,x} = \hat{\mathbf{x}} \gamma_m / (\omega \varepsilon_0 n^2) H_m$. Second, the unconjugated orthogonality in Equation (S27) is applied to Equation (S44) such that the mode expansion coefficient C_m is determined by

$$C_m \times \frac{1}{2}\int_{-\infty}^{\infty} E_{m,x}(x)H_m(x)dx = \frac{1}{2}\int_{-\infty}^{\infty} E_x(x)H_m(x)dx, \quad \text{(S45)}$$

where E_x is the x component of **E**. Last, the power of the mode of order m, P_m at the position is given by

$$P_m = |C_m|^2 \times \frac{1}{2}\mathrm{Re}\left[\int_{-\infty}^{\infty} E_{m,x}(x)H_m^*(x)dx\right], \quad \text{(S46)}$$

where the asterisk * means complex conjugation. P_m is normalized to the input fundamental TM mode power.

S5. Relations of the coupling wavelength to Λ_1 and Λ_2

For the initial values of Λ_1 and Λ_2, determined by the π phase difference condition, the transmission spectrum calculated by using the FDTD method is centered at a wavelength of 7.823 μm. If Λ_1 and Λ_2 are appropriately increased, the transmission spectrum can be made centered at a wavelength of 8 μm. For this purpose, using the mode matching method, we calculated the transmission spectrum with Λ_1 changed between 48 nm and 58 nm but with Λ_2 set at 87 nm. Then, the center wavelength λ_c of the major rejection band in the transmission spectrum was determined. The relation of the center wavelength to Λ_1 is shown in Figure S6a together with the straight line fitted to the relation. The slope of the straight line, $\partial\lambda_c/\partial\Lambda_1$ is 40 nm/nm. Next, we calculated the transmission spectrum with Λ_2 changed between 82 nm and 92 nm but with Λ_1 set at 55 nm. The relation of λ_c to Λ_2 in this case is shown in Figure S6b, and the slope of the straight line fitted to the relation, $\partial\lambda_c/\partial\Lambda_2$ is 25 nm/nm. We confirmed the values of $\partial\lambda_c/\partial\Lambda_1$ and $\partial\lambda_c/\partial\Lambda_2$ determined by using the mode matching method with those determined by using the FDTD method. For this purpose, using the FDTD method we calculated the transmission spectrum for Λ_1 between 48 nm and 58 nm and Λ_2 = 87 nm or for Λ_2 between 82 nm and 92 nm and Λ_1 = 55 nm. To reduce calculation time, the number of periods was set at 10. Figure S6c and Figure S6d show the calculated transmission spectra. The relations of λ_c to Λ_1 and Λ_2 determined by the FDTD method are shown in Figure S6a and Figure S6b, respectively, along with the straight lines fitted to the relations. The slopes of the straight lines are the same as the values of $\partial\lambda_c/\partial\Lambda_1$ and $\partial\lambda_c/\partial\Lambda_2$ determined by the mode matching method. If both Λ_1 and Λ_2 are increased by 3 nm, λ_c is expected

to increase from 7.823 μm to 8.018 μm. Therefore, Λ_1 and Λ_2 are adjusted to be 58 nm and 90 nm, respectively.

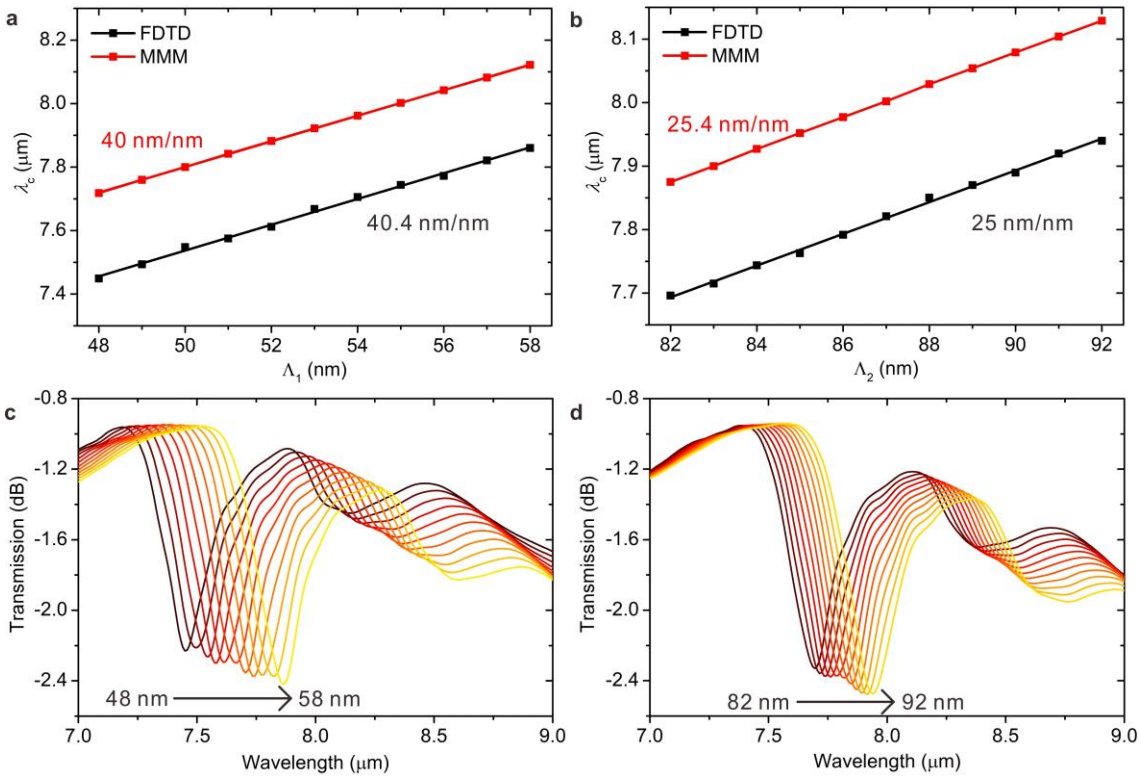

Figure S6. Transmission characteristics depending on Λ_1 and Λ_2. (a) Relations of the coupling wavelength λ_c to Λ_1 for Λ_2 set at 87 nm. (b) Relations of the coupling wavelength λ_c to Λ_2 for Λ_1 set at 55 nm. In panels a and b, the symbols show the relations calculated by using the mode matching method (MMM) and the FDTD method (FDTD). The straight lines are fitted to the relations. (c) Transmission spectra for Λ_1 between 48 nm and 58 nm and Λ_2 = 87 nm. (d) Transmission spectra for Λ_2 between 82 nm and 92 nm and Λ_1 = 55 nm. The transmission spectra were calculated by using the FDTD method for the modulator with the grating with 10 periods.

S6. Change of the transmission spectrum depending on the number of periods

Using the FDTD method, we calculated the transmission spectrum with the number of periods changed from 2 to 40. The calculated transmission spectra are shown in Figure S7a. The center wavelength of the major rejection band almost does not change, and its depth increases with the number of periods. The relation of the transmission at the center wavelength to the number of periods is shown in Figure S7b.

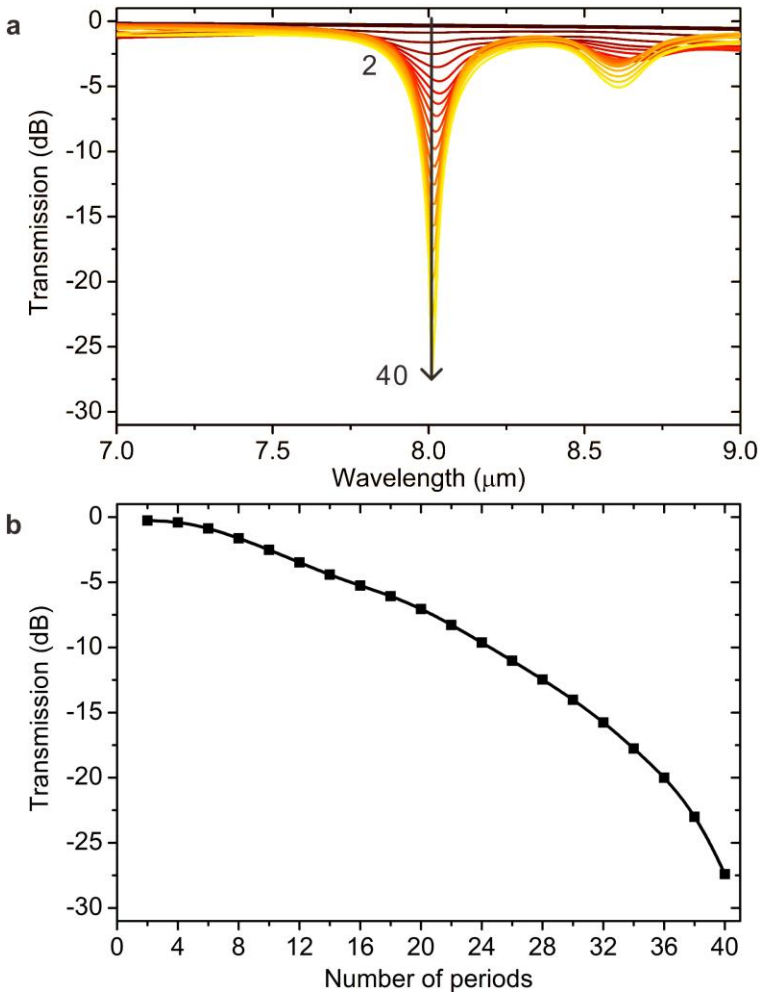

Figure S7. Transmission characteristics depending on the number of periods. (a) Transmission spectra for the number of periods between 2 and 40. (b) Transmission at the coupling wavelength vs. the number of periods.

S7. Power changes of the HPWM and the GPWM in the grating region

The curve calculated by Equation (S5) was fitted to the relation of the normalized power of the HPWM to z, which was calculated by using the FDTD method. In this fitting process, we assumed that α_b is much larger than α_a such that $\bar{\alpha} = \alpha = \alpha_b$. The fitting process resulted in $\bar{\alpha} = \alpha$ = 0.5627 μm^{-1} and $\bar{\kappa}$ = 0.4792 μm^{-1}. The fitted curve is shown in Figure S8a. Then, the curve calculated by Equation (S6) was fitted to the relation of the normalized power of the GPWM to z, which was calculated by using the FDTD method. The fitting process resulted in $\bar{\alpha}$ = 0.4104 μm^{-1} and $\bar{\kappa}$ = 0.5549 μm^{-1}. The values of $\bar{\alpha}$ are close to the attenuation coefficients of the GPWM in

sections 1 and 2, which are 0.6868 μm^{-1} and 0.4807 μm^{-1}. The fitted curve is shown in Figure S8b. For the fitted curves in Figure 3e, the average of the two values of $\bar{\alpha}$ (i.e., 0.4865 μm^{-1}) and the average of the two values of $\bar{\kappa}$ (i.e., 0.5157 μm^{-1}) were used.

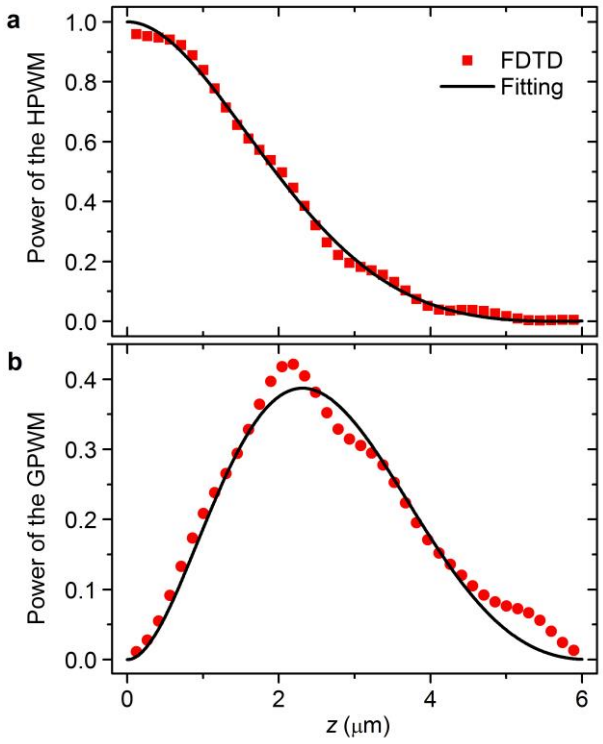

Figure S8. (a) Relation of the HPWM power to z. The curve calculated by Equation (S5) is fitted to the relation calculated by using the FDTD method. (b) Relation of the GPWM power to z. The curve calculated by Equation (S6) is fitted to the relation calculated by using the FDTD method.

S8. Transmission spectra calculated for d_g between 10 nm and 130 nm

We calculated the propagation constant β_{G2} of the GPWM in section 2 as a function of d_g at a wavelength of 8 μm. As shown in Figure S9a, β_{G2} decreases as d_g increases up to 60 nm and does not change so much for d_g larger than 70 nm. Figure S9b shows the transmission spectra calculated for d_g between 10 nm and 130 nm. The relations of the coupling wavelength λ_c and the transmission at λ_c to d_g were obtained from the spectra and used for Figure 4a.

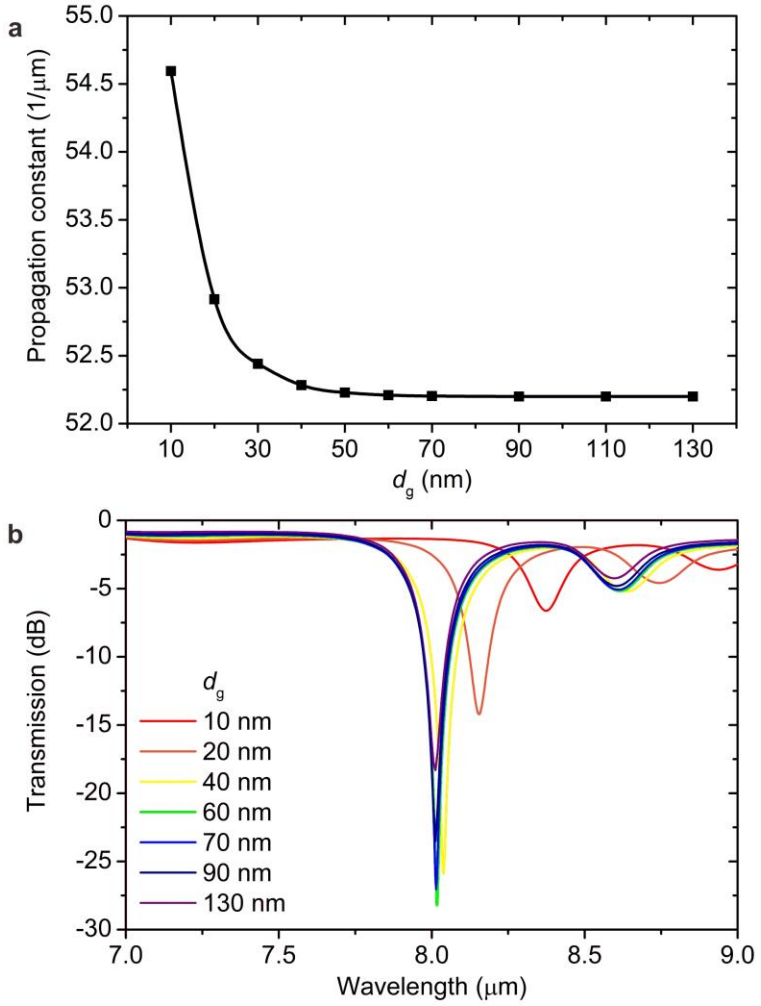

Figure S9. Transmission characteristics depending on the grating depth d_g. (a) Propagation constant β_{G2} of the GPWM in section 2 as a function of d_g at a wavelength of 8 μm. (b) Transmission spectra calculated by using the FDTD method for d_g between 10 and 130 nm.

S9. Transmission coefficient from the HPWM in section 1 to the GPWM in section 2

The transmission coefficient t_{GH} from the HPWM in section 1 to the GPWM in section 2 can be calculated by using Equation (S28). In the calculation, sections 1 and 2 correspond to the left and right waveguides in Figure S3, respectively. The calculated transmission coefficient is shown with respect to d_g in Figure S10. The relation between t_{GH} and the coupling coefficient κ in Supplementary Information S1 is roughly given by $\kappa = 2\sin^{-1} t_{GH} / \Lambda$, where Λ is the grating period. When t_{GH} is around 0.035, κ is approximately 0.47 μm^{-1}.

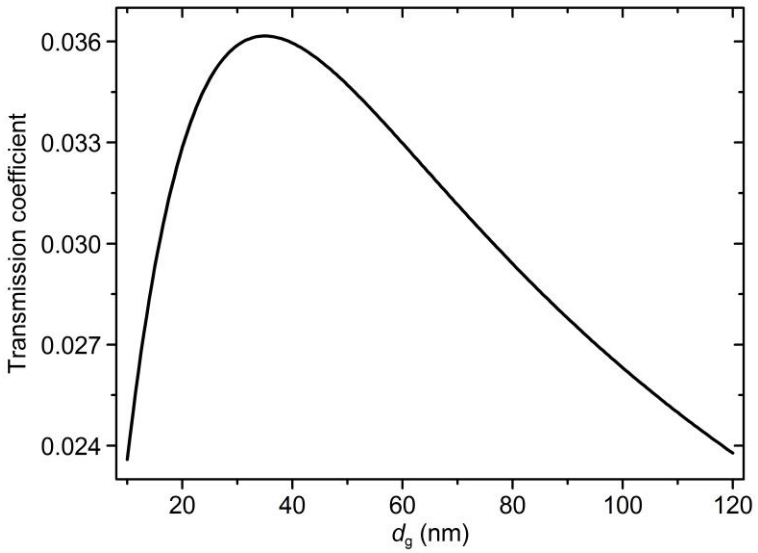

Figure S10. Transmission coefficient from the HPWM in section 1 to the GPWM in section 2 vs. the grating depth d_g.

S10. Transmission spectra calculated for different graphene carrier mobilities

Figure S11a shows the real and imaginary parts of the graphene conductivity as functions of the graphene mobility μ at a wavelength of 8 μm. Figure S11b shows the propagation constants and losses of the GPWM in sections 1 and 2 as functions of μ at a wavelength of 8 μm. Finally, Figure S11c shows the transmission spectra calculated for μ between 1,250 $cm^2/V/s$ and 10,000 $cm^2/V/s$. In the calculations related to all the panels, the chemical potential was set to 0.6 eV.

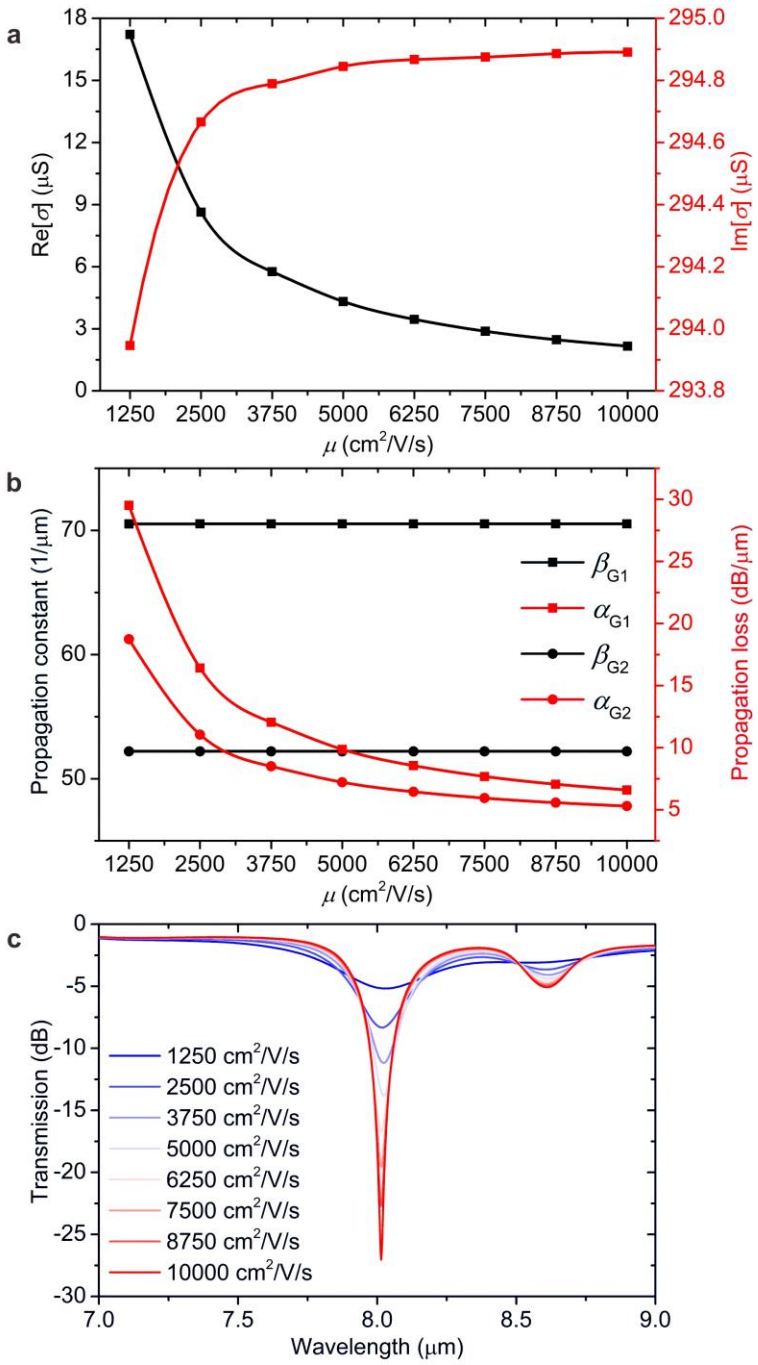

Figure S11. Transmission characteristics depending on the graphene carrier mobility μ. (a) Real and imaginary parts of the graphene conductivity as functions of the graphene mobility μ. (b) Propagation constants and losses of the GPWM in section 1 and 2 as functions of μ. The calculations for panels a and b were done at a wavelength of 8 μm. (c) Transmission spectra for μ between 1,250 and 10,000 cm^2/V/s.

S11. Transmission spectra calculated for μ_c between 0.45 eV and 0.75 eV

Figure S12 shows the transmission spectra calculated for μ_c between 0.45 eV and 0.75 eV. In the calculation, the graphene carrier mobility μ was set to 10,000 $cm^2/V/s$.

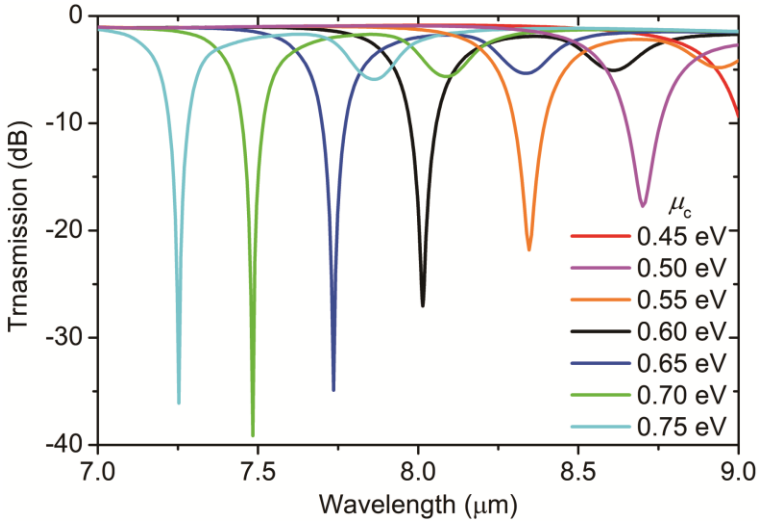

Figure S12. Transmission spectra for μ_c between 0.45 eV and 0.75 eV.

Movie S1. Co-directional coupling between the HPWM and the GPWM

The movie was taken at a wavelength of 8.014 μm for the grating with 15 periods. It can be observed that the GPWM is generated in the right part of the grating and propagating in the hybrid plasmonic waveguide after the grating.

Movie S2. Contra-directional coupling between the HPWM and the GPWM

The movie was taken at a wavelength of 8.62 μm for the grating with 15 periods. It can be observed that the GPWM is generated in the left part of the grating but not propagating rightwards after the grating. There is the weak GPWM propagating leftwards before the grating.

References

S1. Bienstman P, Rigorous and efficient modelling of wavelength scale photonic components (Ph.D dissertation). University of Ghent, Belgium, 2001.